The features of structural transformations in lanthanum manganites La 1−x A x MnO 3+δ (A = Ca, Sr, Ba)

Vera D. Sedykh

Citation: AIP Conference Proceedings **1622**, 72 (2014); doi: 10.1063/1.4898613
View online: http://dx.doi.org/10.1063/1.4898613
View Table of Contents: http://scitation.aip.org/content/aip/proceeding/aipcp/1622?ver=pdfcov
Published by the AIP Publishing

The Features of Structural Transformations in Lanthanum Manganites $La_{1-x}A_xMnO_{3+\delta}$ (A = Ca, Sr, Ba)

Vera D. Sedykh[a)]

Institute of Solid State Physics, Russian Academy of Sciences, Chernogolovka, Russia

[a)] Corresponding author: sedykh@issp.ac.ru

Abstract. In this work, the effect of the ionic radius and concentration of a doping element on the features of the structural transformations in polycrystalline lanthanum manganites, $La_{1-x}A_xMnO_{3+\delta}$ (A = Ca, Sr, Ba), has been studied by Mössbauer spectroscopy and X-ray diffraction analysis. For Mössbauer investigations, a small amount of ^{57}Fe (2 at%) Mössbauer isotope was introduced into the samples. It follows from the analysis of the obtained data that both common features of the structural transformations and differences between them exist in lanthanum manganites depending on ionic radius and concentration of a doping element.

Keywords: Lanthanum manganites, Mössbauer spectroscopy, X-ray diffraction.
PACS: 61.05.cp, 61.05.Qr, 61.50.Ks, 75.47.Lx, 76.80.+y.

INTRODUCTION

Lanthanum manganites doped with a divalent element have a colossal magnetoresistance (CMR) [1–3], and therefore, they are widely used in different fields of techniques. Lanthanum manganites are also used as cathode materials in fuel energetics, since they have a high electron-ionic conductivity. They are the most interesting objects among the oxide family for scientific investigations, since in the system of perovskite compounds, the structural, magnetic, and electron properties are strongly related to each other [4].

As a rule, their structure is studied by X-ray diffraction (XRD). The important information on a local change in atomic environment within a lattice can be obtained by Mössbauer spectroscopy. However, these investigations are very rare [5–7]. By varying syntheses and heat treatment conditions, it is possible to obtain a series of structural modifications the main of which are rhombohedral (space group *R-3c*) and three orthorhombic *PnmaI, PnmaII**, and *PnmaII* (common space group *Pnma*) phases [8,9].

All lanthanum manganites have both common features of structural transformations and differences between them. The first common character belonging to all lanthanum manganites is a mixed Mn valence: Mn^{3+} and Mn^{4+}. Mn^{3+} ions are the Jahn-Teller ions with degenerated orbital states of electrons [10]. In the compounds with the Jahn-Teller ions, the orbital ordering exists. It gives rise to strong lattice distortions and reduced crystal symmetry. Each phase has the definite concentration range of Mn^{4+} ions [11]. Appearance of Mn^{4+} ions (not Jahn-Teller ions) leads to the breaking of orbital ordering and, consequently, to the decrease in lattice distortions and enhancement of crystal symmetry [12 14]. In this case, the structure with a reduced crystal symmetry (*PnmaII* phase, Mn^{4+} ions are absent) transfers to that with a higher crystal symmetry (*PnmaI* phase, Mn^{4+} ions are present). The principal feature of lanthanum manganites with the Jahn-Teller ions involves a strong correlation between lattice and electron subsystems; therefore, the changes in a structure result in significant changes in physical properties (transport and magnetic) [4].

The next important common character is interstitial oxygen strongly affecting the structural, magnetic, and transport properties of manganites. In the parent compound, $LaMnO_{3+\delta}$, a part of Mn^{3+} ions can transfers to Mn^{4+} and excess oxygen coming with Mn^{4+} occupies the interstitial positions in a lattice, since the lattice positions are already occupied [15]. Interstitial oxygen is much more mobile than lattice oxygen and can easy come and leave a

Mossbauer Spectroscopy in Materials Science - 2014
AIP Conf. Proc. 1622, 72-80 (2014); doi: 10.1063/1.4898613

lattice under certain heat treatment conditions. We have previously revealed on the investigation of the parent compound, $LaMnO_{3+\delta}$, that there are reversible structural transitions *PnmaI* ↔ *PnmaII* ↔ *R-3c* under annealing in a vacuum and in air and, namely, interstitial oxygen is responsible for reversibility of these transitions [15]. Moreover, interstitial oxygen distorts the nearest environment of Mn (Fe) ions in the lattice.

Distortions related to interstitial oxygen are clearly detected in the *R-3c* phase of the parent compound [15]. In this phase, Mn has a symmetrical oxygen environment and, hence, the Mössbauer spectrum shows a single line or at least a doublet with a very small Δ value. This is true for the model structure without any interstitial oxygen. In real case, the Δ value is rather large, since this phase has a maximal quantity of Mn^{4+} ions and, consequently, interstitial oxygen which distorts the lattice.

The reasons for the lattice distortions are different for different phases. Lattice distortions are related to interstitial oxygen in the rhombohedral and orthorhombic *PnmaI* phases ($\delta > 0$) and to the Jahn-Teller effect in the *PnmaII* phase, since in this phase, interstitial oxygen is absent ($\delta = 0$) and Mn^{3+} ions exist only.

Numerous experimental investigations on the doped lanthanum manganites showed very complicated and, sometimes, contradictory picture of the interaction of charge, orbital and spin ordering in them. On doping, a divalent element substitutes a trivalent La ion, and, as a consequence, vacant oxygen sites appear in the lattice. As follows from our investigations, a part of Mn^{3+} ions in doped lanthanum manganites transfers to Mn^{4+} during synthesis in air, and oxygen atoms coming with Mn^{4+} firstly occupy these vacant oxygen sites in the lattice and then interstitial positions. The quantity of interstitial oxygen is related to that of Mn^{4+} ions. The quantity of Mn^{4+} ions should increase when increased the quantity of a doping divalent element, and the quantity of interstitial oxygen should decrease, since a part of oxygen ions coming with Mn^{4+} occupies vacant lattice positions. In this case, lattice distortions related to interstitial oxygen decrease.

In the doped lanthanum manganites of a stoichiometric composition, when interstitial oxygen is absent ($\delta = 0$), the quantity of Mn^{4+} ions is equal to that of the doping element. This means that the single *PnmaII* phase in doped lanthanum manganites must not be formed, since this phase must have only Mn^{3+} ions.

Thus, the doping allows to vary the Mn^{3+}/Mn^{4+} ratio and to change the structural modifications. On doping, one more important character appears, *i.e.*, an ionic radius of a doping element which can affect the structural transformations.

In the present work, the effect of a type (ionic radius) and concentration of a doping divalent element on the features of structural transformations in polycrystalline lanthanum manganites, $La_{1-x}A_xMnO_{3+\delta}$ (A = Sr, Ca, and Ba), has been studied by ^{57}Fe Mössbauer spectroscopy and XRD. Sr has almost the same ionic radius (1.13 Å) as La (1.15 Å), the Ca ionic radius (0.99 Å) is smaller and the Ba ionic radius (1.35 Å) is larger than that of La [16].

EXPERIMENTAL DETAILS

$La_{1-x}A_xMnO_{3+\delta}$ polycrystalline powder samples doped with a divalent impurity (A = Ca, Sr, Ba) were synthesized by a sol-gel method. For Mössbauer investigations, the ^{57}Fe (2 at%) Mössbauer isotope was introduced into the samples during synthesis. The synthesis is described in details in [17]. Relation of Mn^{3+} and Mn^{4+} valence states was determined by iodometric titration. XRD analysis was performed using a SIEMENS D500 diffractometer (Cu K_α radiation).

The ^{57}Fe Mössbauer spectra were measured at room temperature using a conventional MS1101 Mössbauer spectrometer operating in a constant acceleration mode and equipped with a $^{57}Co(Rh)$ source of γ-rays. The values of the derived hyperfine Mössbauer parameters are referred to the metallic iron (α-Fe) at room temperature.

RESULTS AND DISCUSSIONS

XRD Data

According to the X-ray data, the synthesized polycrystalline samples with a wide concentration range of the doping element are single-phased and have rhombohedral *R-3c* structure, except for the two Ca-doped samples with $x = 0.20, 0.30$, which have the orthorhombic *PnmaI* structure. The orthorhombic phases of the investigated doped compounds were obtained either during synthesis or by annealing of the synthesized samples at 650 °C and in vacuum.

We have previously shown for the $LaMnO_{3+\delta}$ parent compound [12] that the transition from one to another orthorhombic phase (the quantity of Mn^{4+} ions changes) is accompanied by the appearance of the additional orthorhombic *PnmaII** phase which is not independent and appears only together with emergence of other orthorhombic phase.

The lattice parameters for all the phases of the doped lanthanum manganites are listed in Table 1. The typical XRD patterns for the *PnmaI*, *PnmaII*, and *R-3c* phases are shown in Fig. 1. The reduced crystal symmetry leads to splitting of some reflections in the XRD pattern (*PnmaII* as compared to *PnmaI*).

TABLE 1. Lattice parameters for the *R-3c*, *PnmaI*, and *PnmaII** phases of $La_{1-x}A_xMn_{0.98}Fe_{0.02}O_{3+\delta}$. For comparison, the data for the parent $LaMnO_{3+\delta}$ compound with 1.5 at% ^{57}Fe Mössbauer isotope are listed as well [12]. For the two-phase samples, a quantity of each phase is listed in the last column.

	***a*, Å**	***b*, Å**	***c*, Å**	***V*, Å^3**
***x*, Sr**		***R-3c***		
0.00	5.523(2)		13.326(4)	352.1(3)
0.05	5.522(2)		13.343(4)	352.4(3)
0.10	5.522(2)		13.347(4)	352.5(3)
0.20	5.522(2)		13.360(4)	352.5(3)
***x*, Sr**		***PnmaI***		
0.00	5.523(2)	7.787(3)	5.537(2)	238.1(3)
0.05	5.528(2)	7.789(3)	5.546(2)	238.4(3)
0.10	5.535(2)	7.785(3)	5.548(2)	239.1(3)
***x*, Sr**		***PnmaII, PnmaII****		
0.00	5.725(2)	7.703(3)	5.537(2)	244.5(3)
0.05	5.638(2)	7.729(3)	5.542(2)	241.8(3)
0.10	5.576(2)	7.756(3)	5.541(2)	240.0(3)
***x*, Ca**		***R-3c***		
0.05	5.519(2)		13.322(4)	351.4(3)
0.10	5.517(2)		13.330(4)	351.4(3)
***x*, Ca**		***PnmaI***		
0.05	5.489(2)	7.783(3)	5.515(2)	235.6(3)
0.10	5.492(2)	7.780(3)	5.523(2)	236.0(3)
0.20	5.479(2)	7.753(3)	5,516(2)	234.3(3)
0.30	5.449(2)	7.751(3)	5.482(2)	231.5(3)
0.50	5.425(2)	7.657(3)	5.433(2)	225.7(3)
***x*, Ca**		***PnmaII*, PnmaI***		
0.05	5.681(2)	7.718(3)	5.534(2)	242.9(3)
0.10	5.654	7.721	5.530	241.4
	5.543	7.783	5.530	238.6(25%)
0.20	5.638	7.669	5.484	237.1
	5.521	7.771	5.516	236.7(85%)
***x*, Ba**		***R-3c***		
0.05	5.531(2)		13.369(4)	354.2(3)
0.10	5.541(2)		13.413(4)	356.8(3)
0.20	5.541(2)		13.488(4)	358.7(3)
***x*, Ba**		***PnmaI***		
0.20	5.525(2)	7.844(3)	5.560(2)	241.0(3)
***x*, Ba**		***PnmaII*, PnmaI***		
0.05	5.641	7.757	5.551	242.9
	5.555	7.818	5.575	242.1(47%)
0.10	5.635	7.757	5.561	243.1
	5.552	7.844	5.571	242.6(97%)

During vacuum annealing, when interstitial oxygen leaves the lattice and Mn^{4+} transfers to Mn^{3+}, the synthesized phase transfers to *PnmaI* and then to *PnmaII** phase (for the Sr-doping element) or to a mixture of the two orthorhombic *PnmaII** and *PnmaI* phases (for the Ca- and Ba-doping elements).

The lattice parameters and unit cell volume vary insignificantly in the Sr-doped compounds, significantly decrease in the Ca-doped compounds, and significantly increase in the Ba-doped compounds when the doping element concentration increases (see Table 1 and Fig. 2).

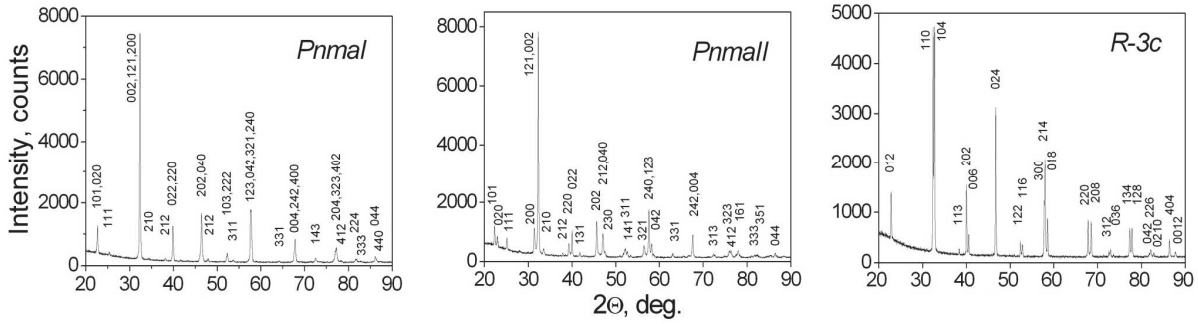

FIGURE 1. Typical XRD patterns of the *PnmaI, PnmaII, and R-3c* phases in lanthanum manganites (Cu $K_{\alpha 1}$ radiation).

The phases are sequentially suppressed on increasing the doping element concentration; finally, the definite single phase is formed for the definite concentration of the doping element; this phase is stable under any heat treatment, *i.e.*, *R-3c* for x(Sr) = 0.2 [18,19] and *PnmaI* for x(Ca) = 0.30 [20].

Since the lattice parameters of the orthorhombic phases are very close to each other, it is quite difficult to separate one phase from another by XRD. This problem can be solved by the employing Mössbauer spectroscopy.

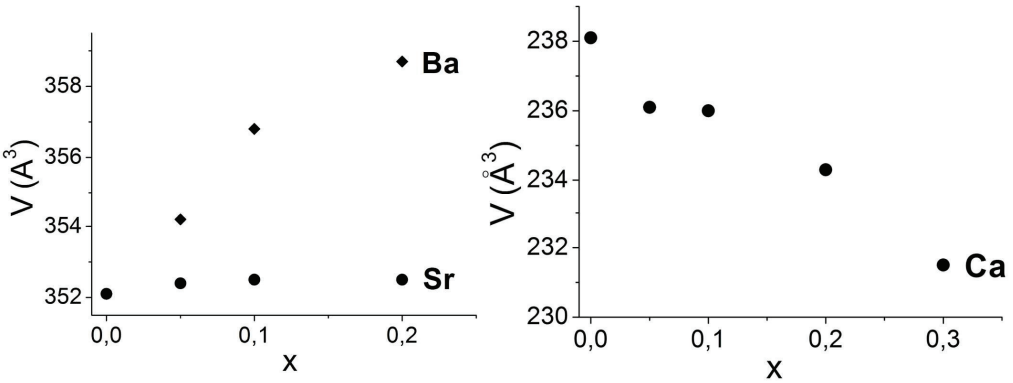

FIGURE 2. Unit cell volume, V, as a function of the doping element concentration, x, for Sr-, Ba- (R-*3c* phase), and Ca- (*PnmaI* phase) doped $La_{1-x}A_xMn_{0.98}Fe_{0.02}O_{3+\delta}$ lanthanum manganites.

Mössbauer Spectroscopy Data

^{57}Fe Mössbauer spectra were measured at room temperature. The hyperfine parameters derived from the Mössbauer spectra for *PnmaI* and *R-3c* phases are listed in Table 2. It follows from the isomer shifts that iron has a trivalent state in all phases of the studied compounds. Fe^{3+} replaces Mn^{3+}. Since Mn^{3+} (0.62Å) and Fe^{3+} (0.62Å) ionic radii are very close to each other, this substitution does not contribute to any structural distortions [21].

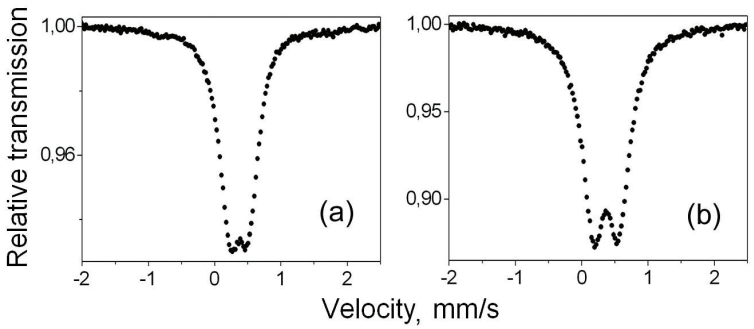

FIGURE 3. Typical Mössbauer spectra for the (a) orthorhombic *PnmaI* and (b) rhombohedral phases in lanthanum manganites.

TABLE 2. Parameters of the room-temperature ^{57}Fe Mössbauer spectra for the *R-3c* and *PnmaI* phases of $La_{1-x}A_xMn_{0.98}Fe_{0.02}O_{3+\delta}$. Δ, *IS*, and Γ are quadrupole splitting, isomer shift, and half-width of line, respectively. *IS* is relative to bcc Fe at room temperature. For comparison, the parameters for the parent compound with 1.5 at% ^{57}Fe are also listed [12].

	Δ ,mm/s	*IS*, mm/s	Γ, mm/s
***x*, Sr**		***R-3c***	
0, 1.5%Fe	0.33(1)	0.37(1)	0.33(1)
0.05	0.31(1)	0.37(1)	0.33(1)
0.10	0.29(1)	0.37(1)	0.33(1)
0.20	0.25(1)	0.37(1)	0.36(1)
***x*, Sr**		***PnmaI***	
0, 1.5%Fe	0.25(1)	0.37(1)	0.34(1)
0.05	0.27(1)	0.37(1)	0.34(1)
0.10	0.27(1)	0.37(1)	0.35(1)
***x*, Ca**		***R-3c***	
0.05	0.31(1)	0.37(1)	0.33(1)
0.10	0.28(1)	0.37(1)	0.34(1)
***x*, Ca**		***PnmaI***	
0.05	0.20(1)	0.37(1)	0.35(1)
0.10	0.23(1)	0.37(1)	0.33(1)
0.20	0.21(1)	0.37(1)	0.34(1)
0.30	0.18(1)	0.36(1)	0.31(1)
0.50	0.14(1)	0.36(1)	0.32(1)
***x*, Ba**		***R-3c***	
0.05	0.32(1)	0.36(1)	0.33(1)
0.10	0.32(1)	0.36(1)	0.33(1)
0.20	0.32(1)	0.36(1)	0.33(1)

Mössbauer spectra for the *R-3c* and *PnmaI* phases are similar for all the studied compounds and shown in Fig. 3. The linewidth of the spectra for these phases is rather narrow (see Table 2) and the spectra were fitted by a single doublet.

As was mentioned above, the quantity of Mn^{4+} ions increases and that of interstitial oxygen decreases on increasing the doping element concentration; therefore, the lattice distortions decrease, which leads to the decrease in the Δ value (see Table 2). Dependence of the Δ value on the doping element concentration for the Ca- and Sr-doped lanthanum manganites is shown in Fig. 4.

It should be noted the following. For the parent compound, the increase in the Mn^{4+} ion concentration leads to the increase in the quantity of interstitial oxygen and to the increase in the lattice distortions related to it. In contrast to the parent compound, the increase in the Mn^{4+} ion concentration in doped lanthanum manganites (related to increasing concentration of the doping element) leads to the decrease in the quantity of interstitial oxygen and, consequently, to the decrease in the lattice distortions related to it.

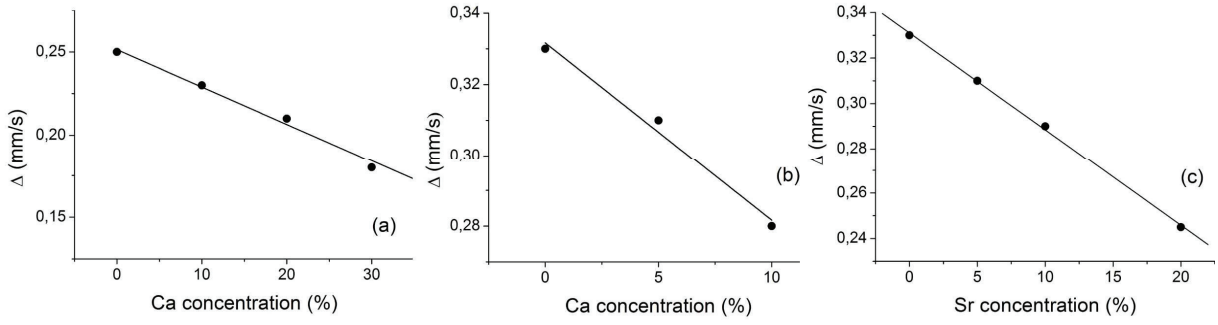

FIGURE 4. Dependence of the Δ value on the doping element concentration for the Ca and Sr-doped lanthanum manganites: (a) *PnmaI* phase, (b) *R-3c* phase, and (c) *R-3c* phase.

In contrast to the *PnmaI* and *R-3c* phases, the Mössbauer spectra for all the investigated compounds with a stoichiometric composition (interstitial oxygen is absent) indicated by XRD data as *PnmaII** or a mixture of two orthorhombic phases display strongly broadened doublets. The broadening of spectrum lines implies that the

spectrum consists of several subspectra. Since the spectra are smooth and do not have any specific feature, it is more correct to fit the spectra by the distribution, $P(\Delta)$, rather than to decompose them into several subspectra. The $P(\Delta)$ distributions for all these spectra were determined using the DISTRI program from the MSTools program complex developed by Rusakov [22,23].

The Mössbauer spectra and the corresponding $P(\Delta)$ distributions for the $La_{1-x}Sr_xMn_{0.98}Fe_{0.02}O_3$ compound of a stoichiometric composition with various Sr concentration are shown in Fig. 5. For comparison, the Mössbauer spectrum and the corresponding $P(\Delta)$ distribution for the parent $LaMnO_3$ compound are also shown in Fig. 5. As it follows from Fig. 5a, the distribution for the parent compound is discrete and has three pronounced peaks. Fe^{3+} is not a Jahn-Teller ion like Mn^{4+}. We have previously shown in the study of the parent compound doped with Fe [24] that Fe^{3+} destroys the orbital ordering like Mn^{4+}, and *PnmaII* transfers to other orthorhombic phases. Each peak corresponds to the definite orthorhombic phase [17,20]. The peak with the largest Δ value corresponds to the *PnmaII* phase with a strongly distorted structure due to the Jahn-Teller effect [6,14], the peak with the smallest Δ value corresponds to the *PnmaI* phase with the enhanced crystal symmetry, and finally, the intermediate peak corresponds to the *PnmaII** phase. For $La_{1-x}Sr_xMn_{0.98}Fe_{0.02}O_3$, the $P(\Delta)$ distribution is rather smooth without any pronounced features [19].

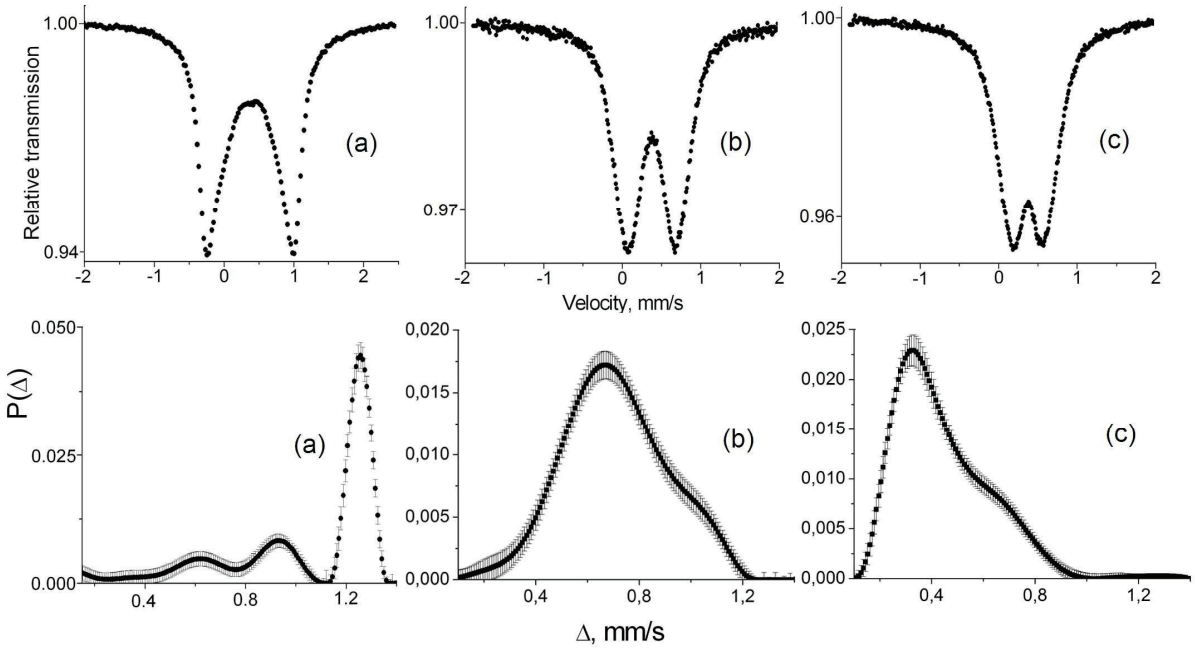

FIGURE 5. ^{57}Fe Mössbauer spectra and corresponding $P(\Delta)$ distributions for $La_{1-x}Sr_xMn_{0.98}Fe_{0.02}O_3$ of a stoichiometric composition for (a) $x = 0$, (b) $x = 0.05$, and (c) $x = 0.10$.

Mössbauer spectra and corresponding $P(\Delta)$ distributions for the Ca- and Ba-doped compounds of a stoichiometric composition are shown in Fig. 6 and Fig. 7, respectively, for different concentrations of the doping element. For these compounds with the Ca and Ba doping elements, the $P(\Delta)$ distributions are discrete with three pronounced peaks. This indicates that all the doped compounds with a stoichiometric composition have three orthorhombic phases instead of one or two orthorhombic phases according to XRD data. The discrete character of the $P(\Delta)$ distribution is most probably caused by the lattice distortions due to a large difference between the La and ionic radii of the doped elements.

Analysis of the distribution shows that the positions of maxima change insignificantly within each phase when changing the type (ionic radius) and concentration of the doping element. This implies that the local environment within each phase changes insignificantly. The strong difference appears only in the change of peak intensities, *i.e.*, in the partial relation of the orthorhombic phases.

Thus, one can say that the mixed valence of Mn ions, *i.e.*, Mn^{3+} (Jahn-Teller ion) and Mn^{4+}, interstitial oxygen, the ionic radius of the doping element, and the lattice distortions related to all these factors are the common factors characterizing the features of the structural transformations in the lanthanum manganites.

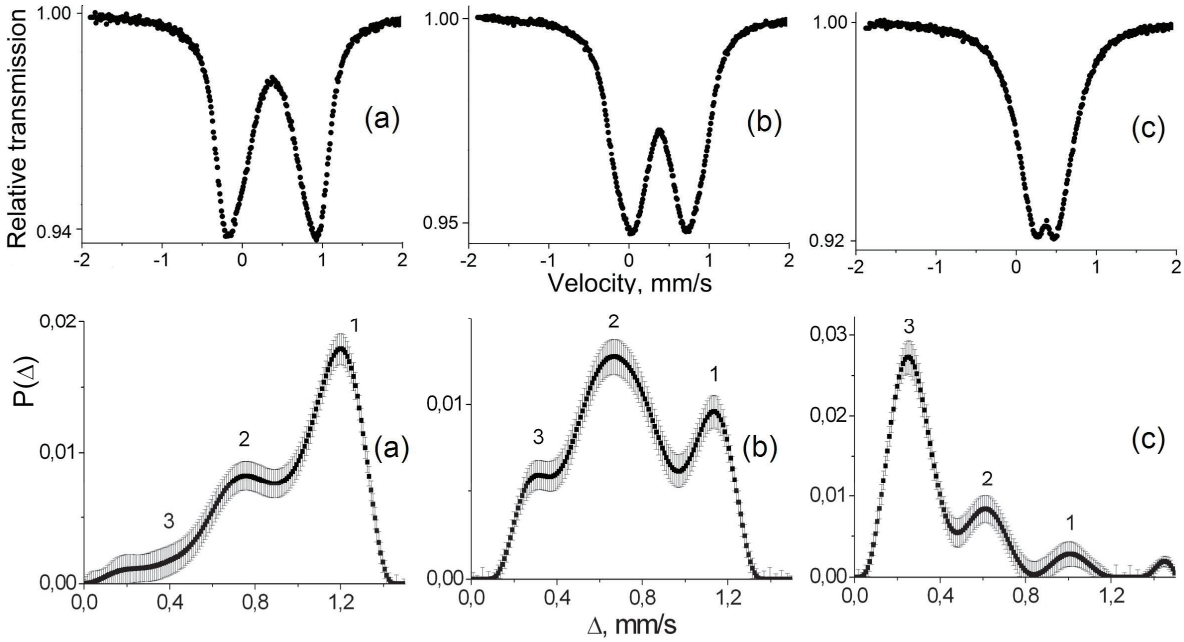

FIGURE 6. ^{57}Fe Mössbauer spectra and corresponding $P(\Delta)$ distributions for $La_{1-x}Ca_xMn_{0.98}Fe_{0.02}O_3$ of a stoichiometric composition for (a) $x = 0.05$, (b) $x = 0.1$, and (c) $x = 0.2$.

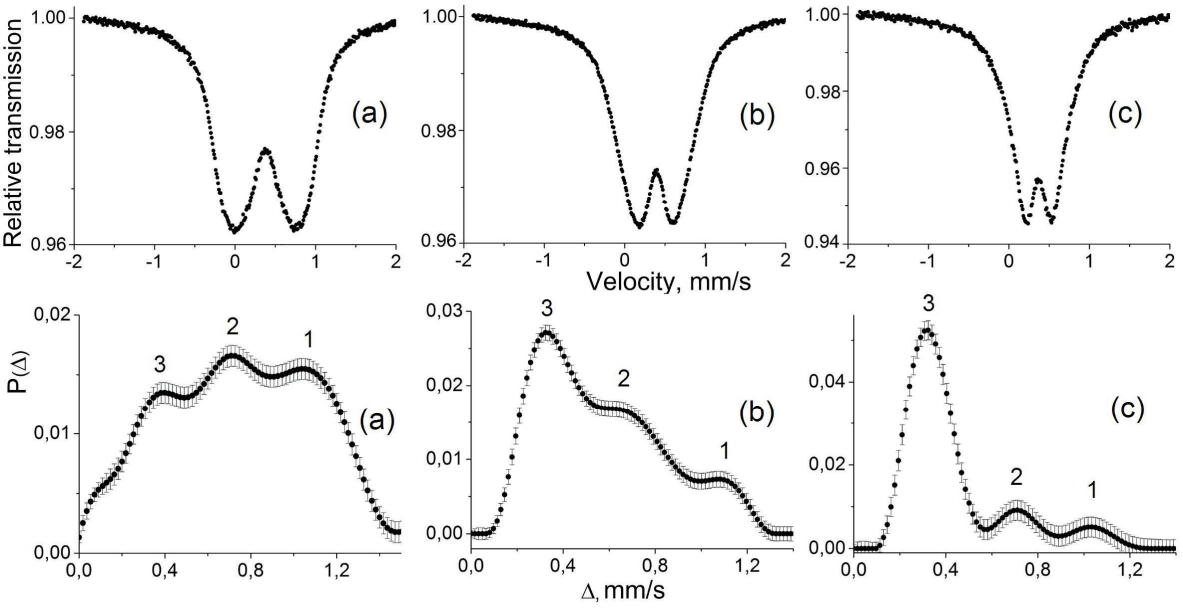

FIGURE 7. ^{57}Fe Mössbauer spectra and corresponding $P(\Delta)$ distributions for $La_{1-x}Ba_xMn_{0.98}Fe_{0.02}O_3$ of a stoichiometric composition for (a) $x = 0.05$, (b) $x = 0.1$, and (c) $x = 0.2$.

Consider the differences in the features of the structural transformations in the doped lanthanum manganites. It follows from the obtained data that the Mössbauer spectra and corresponding $P(\Delta)$ distributions for the studied compounds of a stoichiometric composition with the different type of the doping element strongly differ from each other. Therefore, it is reasonable to compare the distributions for the different compounds with the identical impurity concentration. The $P(\Delta)$ distributions for $x = 0.05$, 0.1, and 0.2 are shown in Fig. 8.

We suppose that the lattice distortions related to the difference in the La and impurity ionic radii most probably slow down the break-down of the orbital ordering in the Ca- and Ba-doped compounds. In the Sr-doped compounds, in which these lattice distortions are absent, the phase suppression occurs faster.

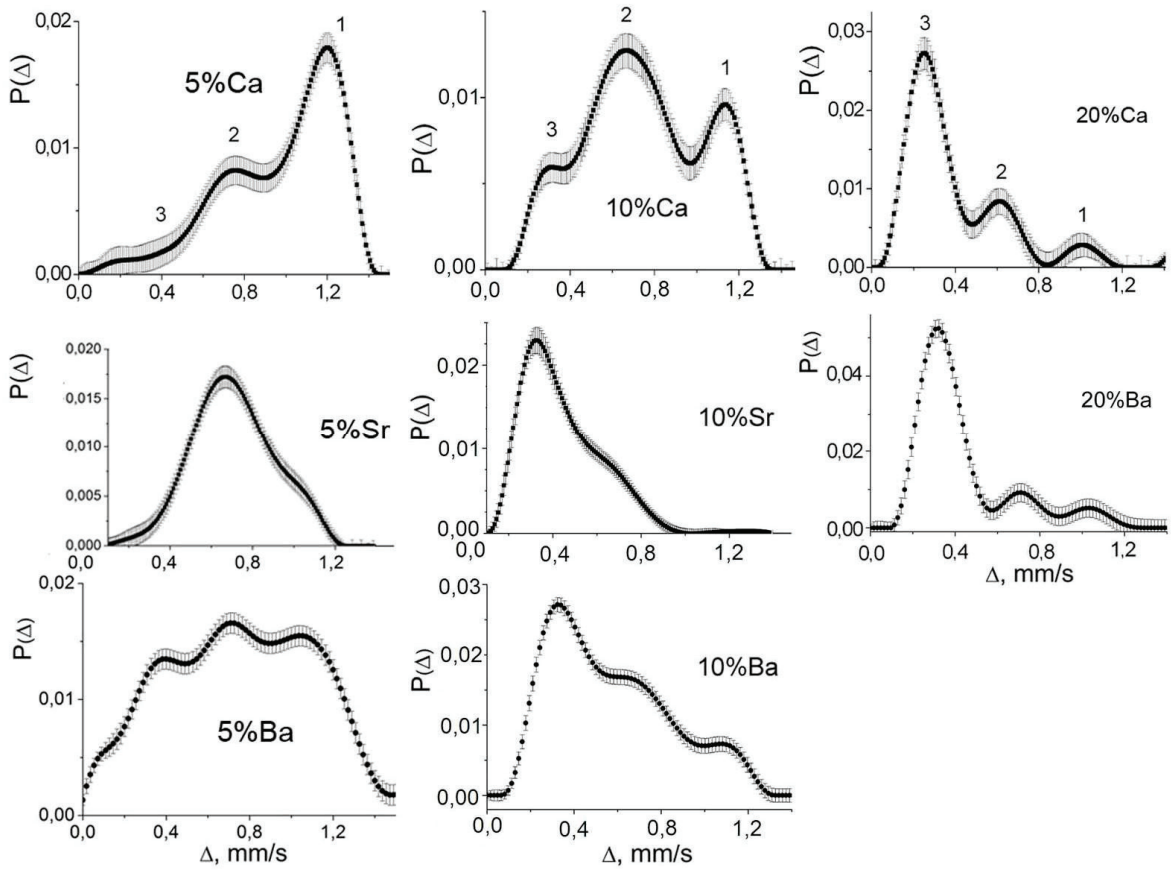

FIGURE 8. Comparison of the $P(\Delta)$ distributions for the different $La_{1-x}A_xMn_{0.98}Fe_{0.02}O_3$ compounds with the identical impurity concentration, $x = 0.05$, 0.10, and 0.20, for the orthorhombic phases.

Distributions for the low concentration of the doping element (x = 0.05 and 0.1) are quite different for the different doping elements. Distributions for the higher concentration of the doping element (x = 0.20) are rather similar. We suppose that the different factors affecting the structural transformations will dominate for the low and higher concentration of the doping element.

As is known from the literature, the change in the ionic radius of the doping element leads to the change in the unit cell volume, in the bond angle of Mn-O-Mn [3,8,25–28], and in the orbital overlapping [29]. This implies that the orbital overlapping is different for the different type of the doping element. By comparing the obtained data, we can suppose that two competing factors exist in the doped lanthanum manganites. One of them is related to the orbital ordering due to the Jahn-Teller effect, the other is related to the appearance of Mn^{4+} ions which destroy the orbital ordering. We assume that for the low concentration of the doping element (x = 0.05 and 0.1), the orbital overlapping is the prevailing factor; for the Ca-doped compounds in which the bond angle of Mn-O-Mn increases, the orbital overlapping is enhanced, whereas for the Ba-doped compounds, the bond angle of Mn-O-Mn decreases and the orbital overlapping decreases, and, therefore, the distributions for the different doping elements are strongly different (see Fig. 7). For the higher concentration of the doping element (x = 0.2), the ratio of Mn^{3+}/Mn^{4+} becomes the prevailing factor and the $P(\Delta)$ distributions for the Ca- and Ba-doped compounds become almost identical.

CONCLUSIONS

By analyzing and comparing the obtained data on the features of the structural transformations in the lanthanum manganites doped with the divalent element, following conclusions can be drawn:

- The structural transformations in the lanthanum manganites have both common characteristic features and differences in the structural transformations.

- At least, the following main factors can affect the structural transformations in the lanthanum manganites: (1) the ratio of Mn^{3+}/Mn^{4+}, (2) interstitial oxygen, (3) ionic radius of the doping element, and (4) the lattice distortions related to all of them. For the different type and concentration range of the doping element, the different factors can dominate. When considering the structural transformations, it is necessary to take into account all these factors.
- Namely, Mössbauer spectroscopy helped investigate in details the features of the structural transformations in the doped lanthanum manganites.

ACKNOWLEDGMENTS

I thank my colleagues for active participation at this work, V. S. Rusakov for fitting the Mössbauer spectra and fruitful discussion of the obtained results, V. Sh. Shekhtman, I. I. Zverkova, and G. E. Abrosimova for XRD analysis, A. V. Dubovitskii for synthesis of the samples, and V. I. Kulakov for the heat treatment of the samples.

The work was made in part under financial support of RFBR grant No. 12-02-00303.

REFERENCES

1. R. Von Hemlolt, J. Wecker, B. Holzapfel, I. Schultz, and K. Samwer, *Phys. Rev. Lett.* **71**, 2331 (1993).
2. V. Podzorov, B. G. Kim, V. Kiryukhin, M. E. Gershenson, and S.-W. Cheong, *Phys. Rev. B* **64**, 140406(R) (2001).
3. A. B. Beznosov, V. A. Desnenko, E. L. Fertman, C. Ritter, and D. D. Khalyavin, *Phys. Rev. B* **68**, 054109 (2003).
4. K. I. Kugel and D. I. Khomskii, *Progr. Phys. Sci*. **136**, 621 (1982).
5. A. Krishnamurthy, B. K. Srivastava, and S. Lokanathan, *Sol. State Commun.* **39**, 983 (1981).
6. M. Pissas and A. Simopoulos, *J. Phys.: Condens. Matter.* **16**, 7419 (2004).
7. D. C. Kundaliya, R. Vij, R. G. Kulkarni, A. A. Tulapurkar, R. Pinto, S. K. Malik, and W. B. Yelon, *J. Magn. Magn. Mater.* **264**, 62 (2003).
8. Q. Huang, A. Santoro, J. W. Lynn, R. W. Erwin, J. A. Borchers, J. L. Peng, and R. L. Greene, *Phys. Rev.* **B 55**, 14987 (1997).
9. V. D. Sedykh, I. S. Smirnova, B. Sh. Bagautdinov, V. Sh. Shekhtman, A. V. Dubovitskii, and V. I. Kulakov, *Surface* **12**, 9 (2002) (*in Russian*).
10. R. Englman, *The Jahn-Teller Effect in Molecules and Crystals*, Wiley-Interscience, New York, U.S.A., 1973.
11. V. D. Sedykh, V. Sh. Shekhtman, I. I. Zver'kova, A. V. Dubovitskii, and V. I. Kulakov, *Bulletin of the Russian Academy of Sciences: Physics* **71**, 1249 (2007).
12. V. Sedykh, G. E. Abrosimova, V. Sh. Shekhtman, I. I. Zver'kova, A. V. Dubovitskii, and V. I. Kulakov. *Physica C* **418**, 144 (2005).
13. J. Rodriguez-Carvajal, M. Hennion, F. Moussa, L. Pinsard, and A. Revcolevschi, *Physica B* **234-236**, 848 (1997).
14. M. Kopcewicz, V. A. Khomchenko, I. O. Troyanchuk, and H. Szymczak, *J. Phys.: Condens. Matter* **16**, 4335 (2004).
15. V. Sedykh, V. Sh. Shekhtman, I. I. Zverkova, A. V. Dubovitskii, and V. I. Kulakov, *Physica C* **433**, 189 (2006**)**.
16. L. T. Bugaenko, S. M. Ryabykh, and A. L. Bugaenko, *Rep. Moscow St. Univ.: Chemistry* **49**, 363 (2008).
17. V. D. Sedykh, V. S. Rusakov, I. I. Zverkova, A. V. Dubovitskii, and V. I. Kulakov, *Phys. Solid State* **54**, 593 (2012**)**.
18. V. D. Sedykh, I. I. Zverkova, V. Sh. Shekhtman, A. V. Dubovitskii, and V. I. Kulakov, *Phys. Solid State* **52**, 591 (2010).
19. V. Sedykh and V.S. Rusakov, "Structural Transformations Features Comparison in $LaMnO_{3+\delta}$ and $La_{1-x}Sr_xMnO_{3+\delta}$ (x = 0.05–0.2)" in *Mössbauer Spectroscopy in Materials Science – 2010*, edited by J. Tuček and M. Miglierini, AIP Conference Proceedings Volume 1258, American Institute of Physics, Melville, New York, U.S.A., 2010, pp. 108-114.
20. V. D. Sedykh, V. S. Rusakov, I. I. Zverkova, A. V. Dubovitskii, and V. I. Kulakov, *Phys. Solid State* **53**, 1440 (2011).
21. H. Ahn, X. W. Wu, K. Liu, and C. L. Chien, *J. Appl. Phys.* **15**, 5505 (1997).
22. V. S. Rusakov, *Bullerin of the Russian Academy of Sciencies: Physics* **7**, 1389 (1999).
23. V. S. Rusakov and K. K. Kadyrzhanov, *Hyperfine Interact.* **164**, 87 (2005).
24. V. D. Sedykh, V. Sh. Shekhtman, A. V. Dubovitskii, I. I. Zverkova, and V. I. Kulakov, *Phys. Solid State* **51**, 351 (2009).
25. Yu. G. Chukalkin and A. E. Teplykh, *Phys. Met. Met. Sci.* **104**, 105 (2007).
26. B. Dabrovski, K. Rogacki, X. Xiong, P. W. Klamut, R. Dybzinski, J. Shaffer, and J. D. Jirgensen, *Phys. Rev. B* **58**, 2716 (1998).
27. P. G. Radaelli, D. E. Cox, M. Marezio, and S.-W. Cheong, *Phys. Rev. B* **55**, 3015 (1997).
28. Q. Huang, J. W. Lynn, R. W. Erwin, A. Santoro, D. C. Dender, V. N. Smolyaninova, K. Ghosh, and R. L. Greene, *Phys. Rev. B* **61**, 8895 (2000).
29. J. F. Jurado and J. A. Jativa, *J. Magn. Magn. Mater.* **335**, 6 (2013).